0026-895X/09/7603-503–515$20.00
MOLECULAR PHARMACOLOGY
Vol. 76, No. 3
56002/3504447
Mol Pharmacol 76:503–515, 2009
Printed in U.S.A.

Hepatic CYP3A Suppression by High Concentrations of Proteasomal Inhibitors: A Consequence of Endoplasmic Reticulum (ER) Stress Induction, Activation of RNA-Dependent Protein Kinase-Like ER-Bound Eukaryotic Initiation Factor 2α (eIF2α)-Kinase (PERK) and General Control Nonderepressible-2 eIF2α Kinase (GCN2), and Global Translational Shutoff[S]

Poulomi Acharya, Juan C. Engel, and Maria Almira Correia

Departments of Cellular & Molecular Pharmacology (P.A., M.A.C.), Pharmaceutical Chemistry (M.A.C.), Biopharmaceutical Sciences (M.A.C.), and Pathology (J.C.E.), the Liver Center (P.A., M.A.C.), and Sandler Center for Basic Research in Parasitic Diseases (J.C.E.), University of California, San Francisco, California

Received March 9, 2009; accepted June 11, 2009

ABSTRACT

Hepatic cytochromes P450 3A (P450s 3A) are endoplasmic reticulum (ER)-proteins, responsible for xenobiotic metabolism. They are degraded by the ubiquitin-dependent 26S proteasome. Consistent with this, we have shown that proteasomal inhibitors *N*-benzoyloxycarbonyl (*Z*)-Leu-Leu-leucinal (MG132) and *N*-benzoyloxycarbonyl-Leu-Leu-Leu-B(OH)$_2$ (MG262) stabilize CYP3A proteins. However, MG132 has been reported to suppress P450s 3A as a result of impaired nuclear factor-κB activation and consequently reduced CYP3A protein stability. Because the MG132 concentration used in those studies was 10-fold higher than that required for CYP3A stabilization, we examined the effect of MG132 (0–300 μM) concentration-dependent proteasomal inhibition on CYP3A turnover in cultured primary rat hepatocytes. We found a biphasic MG132 concentration effect on CYP3A turnover: Stabilization at 5 to 10 μM with marked suppression at $>$100 μM. Proteasomal inhibitors reportedly induce ER stress, heat shock, and apoptotic response. At these high MG132 concentrations, such CYP3A suppression could be due to ER stress induction, so we monitored the activity of PERK [PKR (RNA-dependent protein kinase)-like ER kinase (EIF2AK3)], the ER stress-activated eukaryotic initiation factor 2α (eIF2α) kinase. Indeed, we found a marked ($\approx$4-fold) MG132 concentration-dependent PERK autophosphorylation, along with an 8-fold increase in eIF2α-phosphorylation. In parallel, MG132 also activated GCN2 [general control nonderepressible-2 (EIF2AK4)] eIF2α kinase in a concentration-dependent manner, but not the heme-regulated inhibitor eIF2α kinase [(EIF2AK1)]. Pulse-chase, immunoprecipitation/immunoblotting analyses documented the consequently dramatic translational shutoff of total hepatic protein, including but not limited to CYP3A and tryptophan 2,3-dioxygenase protein syntheses. These findings reveal that at high concentrations, MG132 is indeed cytotoxic and can suppress CYP3A synthesis, a result confirmed by confocal immunofluorescence analyses of MG132-treated hepatocytes.

Hepatic cytochromes P450 (P450s) are endoplasmic reticulum (ER)-anchored integral proteins responsible for the metabolism of various endobiotics as well as xenobiotics, including drugs, toxins, and carcinogens. Of these, human liver CYP3A4 and its mammalian orthologs are noteworthy not only because they biotransform a host of clinically relevant drugs, but also because they are inducible by their substrates via enhanced transcriptional/translational activity, or protein stabilization. Such substrate-mediated regulation of hepatic CYP3A[1] content can result in clinically relevant drug-drug interactions (DDIs), respectively prototyped by the DDIs encountered between rifampin-ethinylestradiol cotherapy on one hand, and grapefruit juice furanocoumarins and felodipine cointake, on the other (Yang et al., 2008). The

This work was supported by the National Institutes of Health National Institute of Diabetes and Digestive and Kidney Diseases [Grant DK26506] and the National Institutes of Health National Institute of General Medicine [Grant GM44037]. We also acknowledge the UCSF Liver Center Core on Cell and Tissue Biology supported by the National Institutes of Health National Institute of Diabetes and Digestive and Kidney Diseases [Grant P30-DK26743].

Article, publication date, and citation information can be found at http://molpharm.aspetjournals.org.

doi:10.1124/mol.109.056002.

[S] The online version of this article (available at http://molpharm.aspetjournals.org) contains supplemental material.

[1] CYP3A or P450s 3A refer to rat liver P450s 3A2, 3A23, 3A18, and 3A9 and/or human liver CYP3A4/CYP3A5.

latter was elegantly documented to be due to furanocoumarin-induced suicidal inactivation of intestinal CYP3A4 and subsequent proteolytic degradation (Lown et al., 1997; Paine et al., 2006).

We have previously reported using various selective probes that native and suicidally inactivated hepatic P450s 3A are turned over via ubiquitin (Ub)-mediated 26S proteasomal degradation (UPD), but not autophagic-lysosomal degradation (ALD), in incubations of freshly isolated hepatocyte suspensions (Wang et al., 1999), cultured primary rat hepatocytes (Faouzi et al., 2007), and in vitro reconstituted CYP3A4 ubiquitination-degradation systems (Korsmeyer et al., 1999). Accordingly, treatment of cultured primary rat hepatocytes with the proteasome inhibitor MG132 or MG262 not only resulted in enhanced profiles of ubiquitinated native and suicidally inactivated CYP3A but also stabilized their hepatic levels (Faouzi et al., 2007). Treatment with the ALD inhibitors 3-methyladenine and NH_4Cl, on the other hand, had little effect on CYP3A turnover. This was experimentally reiterated in *Saccharomyces cerevisiae* wild-type strains and strains with genetic deletions or defects in specific proteins involved in the ER-associated degradation (ERAD) of various integral and luminal ER proteins. Thus, through these genetic yeast screens, the proteolytic degradation of heterologously expressed CYP3A4 was also shown to subscribe to a bona fide ERAD, dependent on UPD but not the vacuolar (ALD) pathway (Murray and Correia, 2001; Liao et al., 2006).

However, several reports have challenged this conclusion and have provided evidence that proteasome inhibitors such as MG132 suppress rather than stabilize CYP3A protein. Although some reports claimed that this suppression is at the mRNA and protein level (Noreault-Conti et al., 2006), others claimed it was due to NFκB-mediated regulation of CYP3A protein stability (Zangar et al., 2008). Accordingly, evidence was provided for a reduced NFκB activation as a result of MG132-mediated inhibition of proteasomal function (Zangar et al., 2008). NFκB activation requires unleashing from its inhibitory IκB regulators via proteasomal degradation. These authors documented that MG132-inhibited proteasomal degradation elevated the cellular levels of some IκB inhibitors but maintained steady-state IκBα levels, thus resulting in a functionally inactive NFκB. This inactive NFκB, the authors proposed, would be incapable of controlling cellular oxidative stress, in turn resulting in CYP3A protein destabilization. Indeed, 6-amino-4-(4-phenoxyphenyl-ethylamino)quinazoline, an NFκB activation inhibitor, was shown to exhibit similar albeit considerably reduced CYP3A4 protein destabilization.

This finding intrigued us primarily because of the 10-fold higher MG132 concentrations (200 μM) used for inhibition of NFκB activation relative to those (10–20 μM) required for proteasomal inhibition. Although we had used similar high concentrations in incubations of freshly isolated hepatocytes (Wang et al., 1999),[2] we had found that these high concentrations were cytotoxic to cultured primary hepatocytes. Indeed, proteasome inhibitors are known to induce ER stress and enhance apoptosis (Bush et al., 1997; Nishitoh et al., 2002; Lee et al., 2003; Jiang and Wek, 2005a). Given this possibility, we explored whether the diametrically opposite MG132 effects observed on CYP3A protein stability could stem from differences in the concentrations employed. We therefore examined the effects of MG132 at concentrations ranging from 0 to 300 μM in cultured primary rat hepatocytes. Our findings described below reveal that MG132 had a biphasic concentration-dependent effect on immunochemically detectable CYP3A levels in cultured rat hepatocytes: stabilization of CYP3A at lower concentrations and a marked suppression at higher concentrations. However, we show that this suppression stems from MG132-induced unfolded protein response (UPR) and consequent ER stress, activation of both PERK [PKR (RNA-dependent protein kinase)-like ER kinase (EIF2AK3)], the resident ER stress-inducible eIF2α kinase, and GCN2 [general control nonderepressible-2 (EIF2AK4)] eIF2α kinase and consequent global suppression of hepatic protein synthesis, and was not due to reduced CYP3A protein stability as reported previously (Zangar et al., 2008). These findings once again underscore the essential role of UPD in CYP3A ERAD, as well as the concentrations of the proteasomal inhibitors critical for its documentation. Given the increasing recognition of proteasomal inhibitors as invaluable therapeutic agents, they are clinically relevant.

Materials and Methods

Materials. Common cell culture medium and supplements such as William's medium E (WME), insulin-transferrin-selenium-G (100×), bovine serum albumin (BSA), penicillin/streptomycin, L-glutamine, liver digestion medium, and liver perfusion medium were obtained from Invitrogen (Carlsbad, CA). Methionine/cysteine-free WME was prepared by the University of California San Francisco (UCSF) Cell Culture Facility (San Francisco, CA). Collagen type I was prepared from frozen rat tails per a protocol established by the UCSF Liver Center Cell and Tissue Biology Core Facility. Matrigel was obtained from BD Biosciences Discovery Labware (Bedford, MA). Petri dishes (60 mm; Permanox) were purchased from Nalge Nunc International (Rochester, NY). Phenylmethylsulfonyl fluoride (PMSF), E-64, antipain, and dexamethasone (Dex) were purchased from Sigma/Aldrich (St. Louis, MO). Sodium vanadate, β-glycerophosphate, and sodium fluoride were obtained from Thermo Fisher Scientific (Waltham, MA). Leupeptin was purchased from Roche Applied Science (Indianapolis, IN); aprotinin, pepstatin A, and bestatin were obtained from MP Biomedicals (Solon, OH). 4-(2-Ami-

[2] Higher concentrations of MG132 were used in these hepatocyte incubations; as a peptide aldehyde, it can be readily quenched by the relatively high GSH concentrations present in these freshly isolated cells.

ABBREVIATIONS: P450, cytochrome P450; ER, endoplasmic reticulum; DDI, drug-drug interaction; Ub, ubiquitin; UPD, ubiquitin-mediated 26S proteasomal degradation; ALD, autophagic-lysosomal degradation; MG132, *N*-benzoyloxycarbonyl (*Z*)-Leu-Leu-leucinal; MG262, *N*-benzoyloxycarbonyl-Leu-Leu-Leu-B$(OH)_2$; ERAD, ER-associated degradation; NFκB, nuclear factor κB; IκB, inhibitor of nuclear factor κB; UPR, unfolded protein response; PERK, PKR-like ER-bound eIF2α-kinase; PKR, RNA-dependent protein kinase; eIF2α, α-subunit of the eukaryotic initiation factor 2; GCN2, general control nonderepressible-2; WME, William's medium E; BSA, bovine serum albumin; UCSF, University of California San Francisco; PMSF, phenylmethylsulfonyl fluoride; Dex, dexamethasone; HRI, Heme-regulated inhibitor; PMSF, phenylmethylsulfonyl fluoride; PAGE, polyacrylamide gel electrophoresis; DAPI, 4,6-diamidino-2-phenylindole; AK, adenylate kinase; TTBS, Tris-buffered saline-Tween 20; TDO, tryptophan 2,3-dioxygenase; PBS, phosphate-buffered saline; HMM, high molecular mass; MEF, mouse embryonic fibroblast; eIF2αP, phosphorylated eIF2α; RHL, rat hepatocyte lysate.

noethyl)benzenesulfonyl fluoride hydrochloride was purchased from Enzo Life Sciences, Inc. (San Diego, CA). MG132 and MG262 were purchased from BostonBiochem (Boston, MA). EasyTag EXPRESS^{35}S-labeled methionine was purchased from PerkinElmer Life and Analytical Sciences (Boston, MA). Rabbit polyclonal IgGs were raised commercially against purified recombinant rat hepatic HRI eIF2α kinase, and purified by Hi-Trap Protein A-Sepharose affinity chromatography.

Animals. Male Sprague-Dawley rats (4–6 weeks old) were purchased from Simonsen Laboratories (Gilroy, CA). Rats were housed at the UCSF Animal Care Facility, fed, and given water ad libitum and handled according to Institutional Animal Care and Use Committee guidelines.

Hepatocyte Isolation and Culture. Hepatocytes were isolated from male Sprague-Dawley rats by in situ liver perfusion with collagenase (liver digest medium) and purified by centrifugal elutriation. Hepatocytes (3×10^6) were seeded onto 60-mm Permanox culture dishes precoated with type I rat tail collagen. Cells were cultured as described previously (Han et al., 2005) in William's E medium containing insulin-transferrin-selenium G, 0.1 μM Dex, 50 U/ml penicillin/streptomycin, 2 mM L-glutamine, and 0.1% BSA. Cells were overlaid with 0.25 mg/ml Matrigel 3 h after plating. Cells were maintained for 2 days with a daily change of medium to enable recovery and cell function restoration and then induced with 20 μM Dex for 3 days (LeCluyse et al., 1999). Treatments were carried out on the fifth day of culture. Cells were treated with vehicle (dimethyl sulfoxide) or MG132 (0, 5, 10, 20, 50, 100, 200, or 300 μM) for 6 h. Cells were harvested in lysis buffer consisting of 20 mM Tris-HCl, pH 7.5, 1% Triton, 150 mM NaCl, 10% glycerol, 1 mM EDTA, 1 mM EGTA, 100 mM NaF, 10 mM tetrabasic sodium pyrophosphate, 17.5 mM β-glycerophosphate, 5 mM *N*-ethylmaleimide, 1 mM Na_3VO_4, and protease inhibitors 1 mM PMSF, 20 μM leupeptin, 1.5 μM aprotinin, 50 μM E-64, 10 μM pepstatin, 10 μM antipain, 1 mM 4-(2-aminoethyl)benzenesulfonyl fluoride hydrochloride, and 60 μM bestatin. The cells were lysed using an Omni-TH homogenizer (Omni International, Marietta, GA) and sonicated for 40 s. Lysates were clarified by sedimentation at maximum speed in a table-top microcentrifuge at 4°C for 15 min. Lysate supernatants were subjected to Western immunoblotting analyses and densitometric quantitation using ImageQuant software (GE Healthcare, Chalfont St. Giles, Buckinghamshire, UK) (see *Immunoblotting Analyses*).

Human Hepatocyte Cultures. Freshly isolated hepatocytes were obtained from CellzDirect (Durham, NC). After a Percoll centrifugation to exclude nonviable cells, they were cultured exactly as described above for cultured rat hepatocytes with rifampicin (15 μM) instead of Dex as the CYP3A4 inducer. On the fifth day of culture, cells were treated with vehicle (dimethyl sulfoxide) or MG262 (0–300 μM) for 6 h and processed exactly as described under *Hepatocyte Isolation and Culture*.

Pulse-Chase Analyses of De Novo CYP3A Synthesis. Hepatocytes were cultured as described above. On the fifth day of culture, cells were treated at time 0, with increasing concentrations of MG132 before the pulse-chase to determine the rate of de novo synthesis of CYP3A after treatment. Five hours thereafter, the culture medium was replaced with Met/Cys-free WME for 1 h containing the MG132 (0–300 μM) and pulsed with 20 μCi/ml of EasyTag EXPRESS^{35}S for 1 h. Each ^{35}S-labeled plate was then washed twice with ice-cold PBS containing excess Met (10 mM) and Cys (1.4 mM). The ^{35}S-labeled protein was chased with 10 mM Met/1.4 mM Cys medium. Lysates were prepared as described under *Hepatocyte Isolation and Culture*. To insure equivalent ^{35}S uptake into hepatocytes, the radioactivity of aliquots of the initial lysate was monitored in Ecolume (4 ml; MP Biomedicals) by liquid scintillation spectrometry using a liquid scintillation counter (LS3801; Beckman Coulter, Fullerton, CA). Aliquots of these lysates were also used for CYP3A immunoprecipitation using 1 mg of lysate protein/3 mg of goat anti-CYP3A IgG. Immunoprecipitates were subjected to SDS-PAGE on a precast 4-to-20% gradient gel. Gels were dried before PhosphorImager analyses. Aliquots of immunoprecipitated ^{35}S-labeled P450s 3A eluates were also subjected to scintillation counting.

Total Hepatic Protein ^{35}S Incorporation. Unlabeled rat liver microsomal protein (10 mg) was added as a protein carrier to ^{35}S-labeled cell lysate protein (1 mg), and the protein was precipitated with 10 volumes of 5% (v/v) H_2SO_4 in methanol followed by at the least five washes with the same solution. Pellets were then washed sequentially with 10 volumes of organic solvents: once with acetone, thrice with ethanol/ether [3:1 (v/v)], and then once with 80% methanol in distilled water. The pellets were air-dried in a biosafety cabinet overnight and dissolved in 1 ml of 1 N NaOH by shaking at 60°C for 5 h, and adjusted to pH 7 to 8 with 2 N HCl, and its protein concentration was determined by the bicinchoninic acid assay. Lysate protein (200 μg) was subjected to liquid scintillation counting for specific radioactivity determination. Total ^{35}S-labeled protein incorporation was calculated as counts per minute per milligram of protein per hour.

Pulse-Chase Analyses of CYP3A Degradation. When the effect of MG132 on CYP3A degradation rate was monitored, cells were cultured as described above. On the fifth day, cells were incubated in a Met/Cys-free medium for 1 h, then pulsed with ^{35}S-Met/Cys for 1 h and chased with cold Met/Cys along with MG132 (0, 10, 20, 200, and 300 μM). Cells were harvested in the lysis buffer at the time of chase (0-time) and at 3 or 6 h thereafter. Lysates prepared as described above were used for CYP3A immunoprecipitation using 1 mg of lysate protein/3 mg of goat anti-CYP3A IgG. Immunoprecipitates were subjected to SDS-PAGE on a precast 4-to-20% gradient gel. Gels were dried before PhosphorImager analyses. Aliquots of immunoprecipitated [^{35}S]CYP3A eluates were also subjected to scintillation counting.

Immunofluorescence Staining. After MG132 (0, 10, 20, 200, and 300 μM) treatment, cells were fixed in methanol for 15 min at −20°C and incubated for 1 h with 2% nonimmune rabbit serum. This was followed by incubation with goat anti-CYP3A antibody [1:500 (v/v)] for 1 h at room temperature. After washing with PBS, cells were incubated with Alexa Fluor 488 rabbit anti-goat antibody [1:3000 (v/v); Invitrogen]. Cells were observed with a confocal microscope (Axiovert 200M, LSM 510 Meta; Carl Zeiss Inc., Thornwood, NY) using a 100×, 1.4 numerical aperture oil objective. Images were collected at 1024 × 1024 frame resolution with a pinhole of 0.75 Airy units. Vectashield mounting medium (Vector Laboratories, Burlingame, CA) with DAPI was added to the culture chambers for DNA staining of hepatic nuclei. The relative nuclear diameters of untreated and MG132 (300 μM)-treated cells (n = 20 each) were determined as an index of apoptotic shrinkage induced by MG132 treatment.

Cell Viability Assay via Trypan Blue Exclusion. Cells were mixed with Trypan Blue dye 1:1 (v/v) and counted on a hemocytometer slide. Triplicate samples of each cell culture were treated with the dye, and each was counted in four quadrants of the slide (12 values for each concentration of MG132 were used to determine the mean ± S.D.). Percentage cell viability was calculated as [(live cells/total cells) × 100].

Cytotoxicity Analyses. A nondestructive luciferase-based bioluminescence ToxiLight assay (Lonza Rockland, Inc., Rockland, ME) was used to monitor any cytotoxicity of cultured hepatocytes induced by MG132 (0–300 μM) concentrations over the 6-h treatment relative to basal 0 μM/0 h levels. This assay monitors the release of intracellular adenylate kinase (AK) into the culture medium, expressed as relative luminescence unit values, wherein the emitted light is directly proportional to the AK activity in the medium. Lysates from untreated cells obtained at 0 h were diluted to the equivalent volume with the cell culture medium and equivalent aliquots used to monitor the total (100%) cellular AK activity available for release into the media. The assay was performed by the manufacturer's instructions exactly as described previously (Han et al., 2005). In parallel, after treatment with either 0 or 200 μM MG132 for 6 h, the medium of some cell cultures was replaced with fresh medium

without MG132, and they were similarly monitored at 24 or 48 h after initial treatment to determine the progression of the cytotoxicity, if any.

DNA Fragmentation Analyses As an Apoptotic Index. In mammalian cells, proteasome inhibition is associated with UPR, eIF2α kinase activation as well as apoptosis (Jiang and Wek, 2005a). To determine the extent of the apoptosis, internucleosomal DNA fragmentation, a hallmark of apoptosis, was monitored in hepatocytes treated with MG132 (0–300 μM) for 6 h using the Quick Apoptotic DNA Ladder Kit obtained from Enzo Life Sciences (Plymouth Meeting, PA) exactly as described in the kit instructions. Total chromosomal DNA was extracted from harvested cells and quantified, and DNA (250 μg) from each treatment group was subjected to 1.2% agarose gel chromatography in the presence of 0.5 μg/ml ethidium bromide. The ethidium-bromide stained DNA ladders were visualized by UV trans-illumination. The medium of some cell cultures treated with MG132 (200 μM) for 6 h was replaced with fresh medium without MG132 and monitored after 24 and 48 h as well to enable the determination of any progression of this effect with time.

Immunoblotting Analyses. Unless specifically stated otherwise, 5% nonfat milk in 0.1% Tris-buffered saline-Tween 20 (TTBS) was

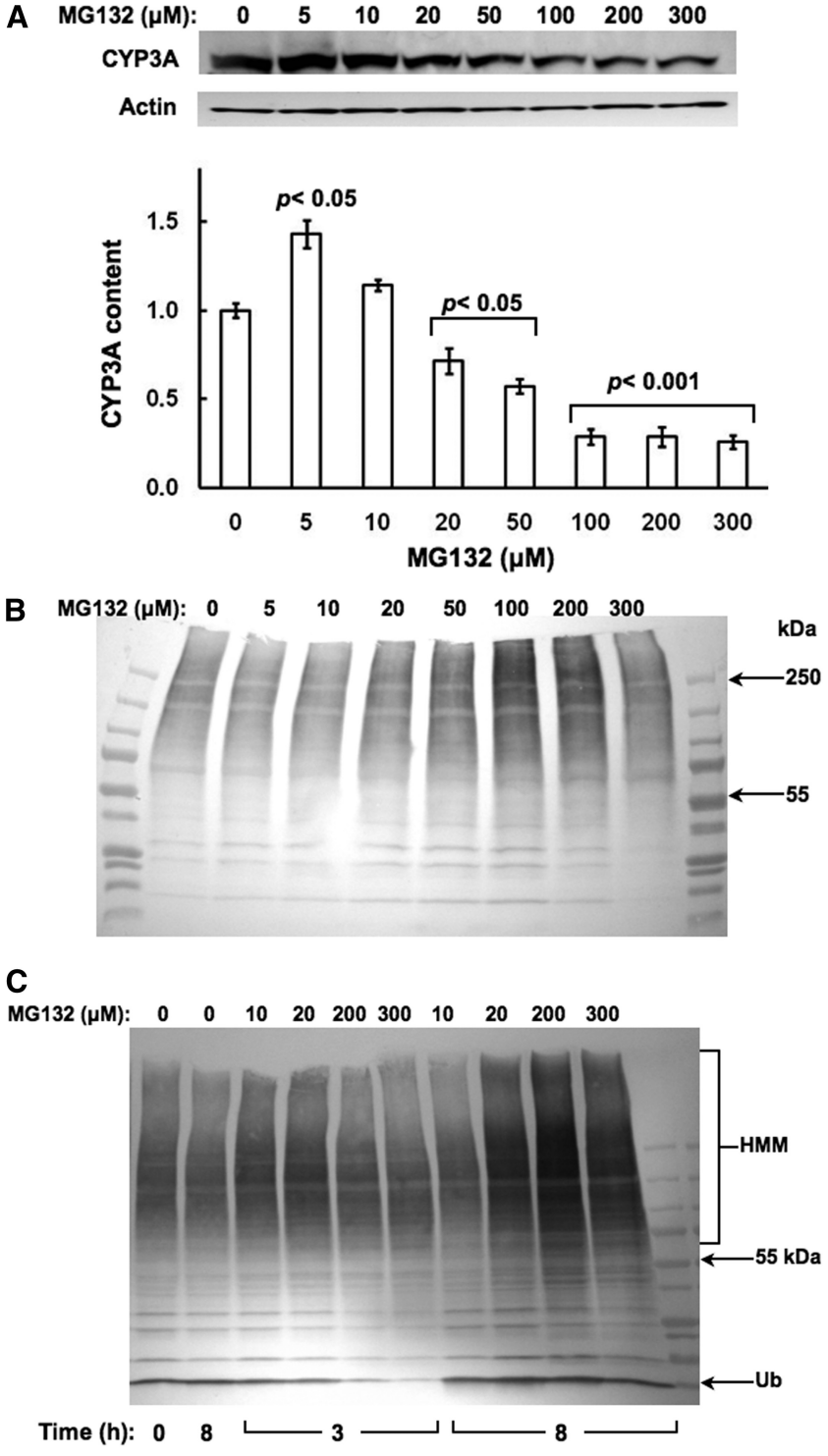

Fig. 1. Concentration-dependent effects of MG132 on CYP3A content in cultured rat hepatocytes. A, rat hepatocyte cultures were treated with 0 to 300 μM MG132 as detailed. A representative example of Western immunoblotting analyses of rat hepatocyte lysate (RHL; 15 μg of protein) from three separate experiments is shown at the top, and the densitometric quantitation of each experiment normalized to the CYP3A content in the corresponding untreated (0 μM MG132) RHL is shown at the bottom. Corresponding RHL aliquots were used for actin immunoblotting analyses as loading controls. Values represent mean ± S.D. of at the least three separate experiments. Statistically significant differences from the untreated value were observed at $p < 0.05$ for the 5 μM, $p < 0.05$ for the 20 and 50 μM, and $p < 0.001$ for the 100 to 300 μM MG132 treatments. B, aliquots of each of these RHLs were used for CYP3A immunoprecipitation, and subsequent Western immunoblotting analyses of the CYP3A immunoprecipitates with an anti-Ub antibody as detailed under *Materials and Methods*. C, relative ubiquitination of total RHL protein at 0, 3, and 8 h, confirming proteasomal inhibition by MG132.

used for blocking and to make all primary and secondary antibody dilutions, and all immunoblots were developed with the SuperSignal West maximum sensitivity Femto or Pico chemiluminescent substrate from Pierce (Rockford, IL). Actin immunoblotting analyses were routinely conducted with each lysate to insure equivalent protein loading. However, because of the low abundance of basal hepatic PERK, GCN2, and HRI protein content, the protein amounts required for their detection by the Femto system greatly exceeded those required for the detection of the relatively more abundant actin protein. The immunoblots were therefore loaded on the basis of the protein concentration of each cell lysate, and the data were normalized based on the immunoblots from lysates harvested at 0 h. In parallel, smaller aliquots (10 μg of protein) of these same SDS-PAGE sample buffer-solubilized cell lysates were subjected to actin immunoblotting analyses to verify that they matched the corresponding bicinchoninic acid assay-determined protein concentrations.

CYP3A, ubiquitinated cellular protein, or ubiquitinated CYP3A protein was immunoblotted as described previously (Correia et al., 2005; Faouzi et al., 2007). eIF2α/eIF2αP, actin, and Grp78/BiP were subjected to immunoblotting analyses as detailed previously (Han et al., 2005). HRI protein and hepatic cytosolic tryptophan 2,3-dioxygenase (TDO) immunoblotting analyses were carried out with primary rabbit polyclonal antibodies against the corresponding recombinant rat hepatic HRI and TDO proteins as described previously (Liao et al., 2007).

PERK. Lysate protein (100 μg) was used for Western immunoblotting. After blocking, the membranes were incubated overnight with a primary rabbit polyclonal antibody raised against the N-terminal 21 to 320 residues of human PERK [1:750 (v:v); Santa Cruz Biotechnology, Santa Cruz, CA] in 4% milk in TTBS. The blots were washed five times with 0.1% TTBS, followed by a secondary goat anti-rabbit IgG-horseradish peroxidase [1:50,000 (v:v); Santa Cruz Biotechnology] in 4% milk in TTBS.

PERK-P. Immunoblotting analyses were identical to those of PERK except that the blocking solution was made of 1% milk, 1% BSA, 0.05% Tween 20 in PBS, and 50 mM NaF (a phosphatase inhibitor). Primary and secondary antibody dilutions were made in this same blocking solution. The primary antibody was a rabbit polyclonal raised against a short amino acid sequence containing phosphorylated Thr981 of human PERK [1:500 (v/v); Santa Cruz Biotechnology]. All washes were carried out with 0.05% Tween 20 and 50 mM NaF in PBS.

The authenticity of the PERK and PERK-P bands was confirmed by treatment of cultured rat hepatocytes with thapsigargin (5 and 10 μM), a well recognized ER stress inducer that is known to induce and autoactivate PERK via phosphorylation. Lysates from commercially obtained SK-N-KH neuroblastoma-cells overexpressing recombinant PERK protein (Santa Cruz Biotechnology) were also included as a positive control.

GCN2. Lysate protein (50 μg) was used for immunoblotting analyses. Membranes were first blocked for 1 h and then incubated with a primary rabbit polyclonal antibody against C-terminal residues 1350 to 1649 of human GCN2 [1:1000 (v/v); Santa Cruz Biotechnology] followed by a goat anti-rabbit horseradish peroxidase-conjugated secondary IgG [1:30,000 (v/v); Bio-Rad Laboratories, Hercules, CA]. The specificity of the commercial anti-GCN2 antibody was confirmed by parallel immunoblotting analyses with a monoclonal antibody raised against a mouse GCN2 carboxyl-terminal domain and kindly provided by Prof. Ronald. C. Wek. Lysates from commercially obtained HeLa cells overexpressing recombinant GCN2 protein (Santa Cruz Biotechnology) were also included as a positive control.

PhosphorImager Analyses/Densitometric Quantitation. The immunoprecipitated [^{35}S]CYP3A was solubilized with 60 μl of SDS-PAGE loading buffer containing 5% SDS, 20% glycerol, 50 mM dithiothreitol, and 5% β-mercaptoethanol in 50 mM Tris buffer, pH 6.8, boiled for 5 min, and then equivalent aliquots (45 μl) were subjected to SDS-PAGE on 4–20% Tris-HCl gels. The gels were then dried and exposed to PhosphorImaging screens and visualized with a Storm PhosphorImager (GE Healthcare). Direct quantification of the radioactive bands in dried gels was performed by ImageJ (http://rsbweb.nih.gov/ij/) analyses. ImageJ was also used for quantification of all the immunoblots.

Statistical Analyses. The Kolmogorov-Smirnov test was used to check whether the data followed normal distribution. Experiments were performed in triplicate. Data were compared by analysis of variance. p values < 0.05 were considered statistically significant.

Results

Concentration-Dependent Effects of MG132 on Hepatic CYP3A Protein Content and Ubiquitination. Immunoblotting analyses with goat anti-rat liver CYP3A23 IgGs of lysates from cultured hepatocytes revealed that treatment with MG132 (0–300 μM) for 6 h resulted in a biphasic effect on CYP3A protein content monitored at 55 kDa: stabilization at lower 5 to 10 μM concentrations, with a marked statistically significant ($p < 0.001$) reduction at concentrations above 100 μM (Fig. 1A). Corresponding CYP3A immunoprecipitation analyses of these lysates followed by immunoblotting analyses with rabbit anti-Ub IgGs revealed a progressively increased level of CYP3A ubiquitination detectable as a characteristic ladder of high molecular mass species (HMM; >75 kDa) (Fig. 1B). This profile intensified at 200 μM MG132 concentrations, before declining thereafter. Parallel immunoblotting analyses of these lysates for total protein ubiquitination revealed a time- and concentration-dependent accumulation of hepatic ubiquitinated proteins, which similarly reached a maximum at 200 μM, before starting to decline (Fig. 1C). These results confirm MG132-induced functional inhibition of the 26S proteasome, and indicate that at the lower concentrations, MG132 indeed stabilizes both the parent (55 kDa) and ubiquitinated (HMM) CYP3A proteins. Similar suppression was also observed with CYP3A4/CYP3A5 in cultured human hepatocytes treated with MG262 (>100 μM), another proteasomal inhibitor that also stabilizes CYP3A (Faouzi et al., 2007) (Fig. 2).

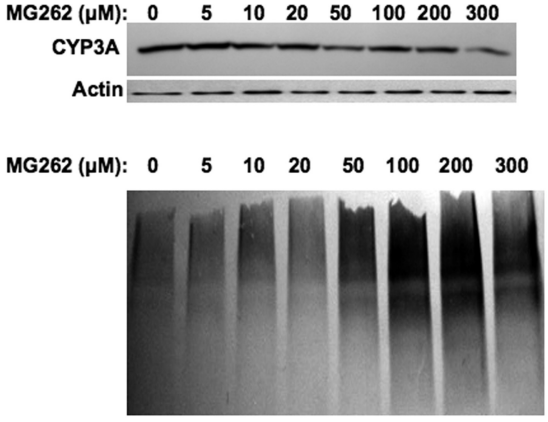

Fig. 2. Concentration-dependent effects of MG262 on CYP3A content in cultured human hepatocytes. Human hepatocyte cultures were treated with 0 to 300 μM MG262 as detailed. A representative example of Western immunoblotting analyses of human hepatocyte lysate (15 μg of protein) is shown at the top, with corresponding aliquots used for actin immunoblotting analyses as loading controls. Aliquots of the lysate (1 mg of protein) were used for CYP3A immunoprecipitation, and subsequent Western immunoblotting analyses of the CYP3A immunoprecipitates were made with an anti-Ub antibody as detailed under *Materials and Methods.* Densitometric quantitation of CYP3A content in hepatocytes treated at various MG262 concentrations relative to basal (1.0) value at 0 μM was as follows: 1.20 (5 μM), 0.92 (10 μM), 0.93 (20 μM), 0.67 (50 μM), 0.77 (100 μM), 0.75 (200 μM), and 0.52 (300 μM).

Concentration-Dependent Effects of MG132 on Hepatic PERK Activation. Because proteasome inhibitors are well recognized inducers of cellular stress in Madin-Darby canine kidney cells as well as mouse embryonic fibroblasts (MEFs) (Bush et al., 1997; Jiang and Wek, 2005a), we probed whether high concentrations of MG132 could similarly induce ER stress in cultured hepatocytes, thereby accounting for the observed CYP3A suppression. We examined the autophosphorylation-mediated activation of PERK, the integral ER stress inducible eIF2α kinase (Harding et al., 2003), as an ER stress marker in hepatocytes treated with MG132 (0–300 μM) for 6 h. PERK activation can be monitored via immunoblotting analyses with an antibody that recognizes a specific phosphorylated PERK epitope, and quantified by monitoring the resulting ratios of densitometrically quantified PERK-P (hyperphosphorylated species) to total PERK content determined with an antibody that recognizes both phosphorylated and unphosphorylated PERK species. Progressive PERK autophosphorylation was observed even at the lowest (5 μM) MG132 concentration, progressively increasing at the higher concentrations (Fig. 3A). Furthermore, in parallel, total PERK content was also increased, possibly as a result of MG132-inducible ER stress (Fig. 3A). The specificity of the commercial antibodies used for immunoblotting analyses of PERK and PERK-P was validated with the use of two positive controls: lysates from hepatocytes treated with thapsigargin, an ER stress inducer, as the positive control for PERK induction/autoactivation, as well as lysates from SK-N-KH neuroblastoma-cells overexpressing recombinant PERK protein (Fig. 3B).

Parallel immunoblotting analyses of Grp78/Bip, the luminal ER-chaperone that is an accepted ER stress marker also revealed a biphasic effect of MG132: a marked 4- to 5-fold Grp78 protein induction over basal levels at the lower (0–50 μM) concentrations, and a progressive decline thereafter at the >100 μM-concentrations in MG132-treated hepatocytes (Fig. 3C). However, even at the highest MG132 concentrations Grp78 content remained somewhat above basal levels.

Concentration-Dependent Effects of MG132 on Other Hepatic eIF2α Kinases. In MEFs, proteasome inhibition is associated primarily with the activation of GCN2 eIF2α kinase rather than PERK (Jiang and Wek, 2005a). To determine whether MG132 had any effects on hepatic GCN2, we monitored its content (Fig. 4). Our findings revealed that in addition to activating hepatic PERK (Fig. 3), MG132

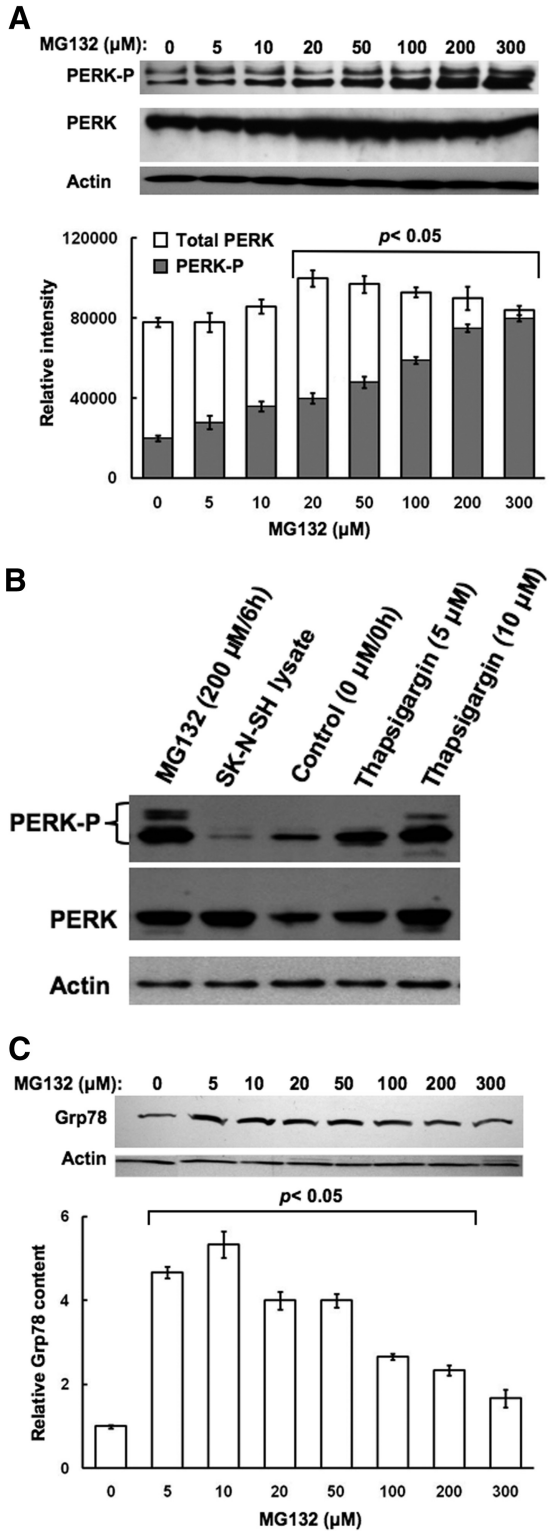

Fig. 3. Concentration-dependent effects of MG132 on induction of PERK content and its autophosphorylation in cultured rat hepatocytes. A, rat hepatocyte cultures were treated with 0 to 300 μM MG132 as detailed. A representative example of Western immunoblotting analyses of RHL from three separate experiments is shown at the top with corresponding aliquots used for actin immunoblotting analyses as loading controls. The densitometric quantitation of the relative PERK-P content (solid bars) to the total PERK immunochemically detectable content (open bars) in each experiment is shown at the bottom. Values represent mean ± S.D. of at the least three separate experiments. Statistically significant differences in PERK-P content and the PERK-P/PERK values were observed at $p < 0.05$ for the 20 to 300 μM MG132 treatments. B, the specificity of the anti-PERK and anti-PERK-P antibodies was verified by immunoblotting analyses against lysates from SK-N-SH human neuroblastoma cells overexpressing PERK (400 ng of PERK protein) and lysates (50 μg) from hepatocytes treated with thapsigargin (5 or 10 μM), a well-known ER stress inducer, as positive controls in immunoblotting analyses of lysates (100 μg of protein) from hepatocytes treated with 0 or 200 μM MG132 as detailed above (A). In parallel, smaller aliquots (10 μg protein) of these same SDS-PAGE sample buffer-solubilized cell lysates were subjected to actin immunoblotting analyses. C, RHL aliquots (50 μg of protein) were also used for monitoring Grp78/BiP immunochemically detectable content. A representative example of Grp78 Western immunoblotting analyses of RHL from three separate experiments is shown at the top, with corresponding aliquots used for actin immunoblotting analyses as loading controls. The densitometric quantitation of the immunochemically detectable Grp78 content in each experiment is shown at the bottom. Values represent mean ± S.D. of at the least three separate experiments. Statistically significant increases over the basal (untreated) content were observed at $p < 0.05$ for 5 to 200 μM MG132 treatments.

showed a marked concentration-dependent increase, not only of hepatic GCN2 content but also of its autophosphorylation, as indicated by the significant appearance of hyperphosphorylated GCN2 species ranging between 150 and <206 kDa (Fig. 4A), as observed with an in vitro-phosphorylated recombinant mouse GCN2 (Berlanga et al., 1999). The specificity of the commercial antibodies used for immunoblotting analyses of GCN2 was validated with the use of a positive control: lysates from HeLa cells overexpressing recombinant GCN2 protein (Fig. 4B). Qualitatively similar findings were also obtained with a monoclonal antibody raised against a mouse GCN2 carboxyl-terminal domain and kindly provided by Prof. Ronald C. Wek (data not shown). Densitometric quantitation of these hyperphosphorylated species as a fraction of the total GCN2 revealed that MG132 resulted in a significant autoactivation of hepatic GCN2 that was indeed dramatic at concentrations >50 μM (Fig. 4A). Comparison of the data in Figs. 3A and 4A reveal that PERK is activated at lower MG132 concentrations than GCN2, thereby revealing its higher sensitivity to proteasomal inhibition.

By contrast, no such increases were detected in hepatic HRI (Fig. 4C), the other heme-regulated eIF2α kinase that is reportedly activated in MEFs by proteasomal inhibition by MG132 or bortezomib (Velcade) (Yerlikaya et al., 2008). Together, these findings in cultured rat hepatocytes indicate that high concentrations of MG132 can activate at the least two hepatic eIF2α kinases.

To determine whether such PERK and GCN2 autophosphorylation was functionally relevant to the liver cell, we monitored their eIF2α kinase activity by examining the levels of phosphorylated eIF2α (eIF2αP) with an antibody that specifically recognizes its phosphorylated epitope relative to total eIF2α content in hepatocytes treated with MG132 (0–300 μM) for 6 h. Our findings revealed a progressive increase in eIF2αP levels relative to unaltered total eIF2α levels with a statistically significant increase in the eIF2αP/eIF2α ratios detected at MG132 concentrations from 100 to 300 μM (Fig. 5).

Concentration-Dependent Effects of MG132 on De Novo Hepatic Total Protein and CYP3A Synthesis. Because eIF2α phosphorylation results in translational arrest of protein synthesis, we determined whether this eIF2α phosphorylation had any physiological relevance to MG132-treated hepatocytes by monitoring their de novo hepatic protein synthesis by pulse-chase analyses after treatment for 6 h at the indicated MG132 concentration. Once again, a concentration-dependent inhibition of total hepatic protein synthesis was detected and was particularly marked at the higher 200 to 300 μM MG132 concentrations tested (Fig. 6A). These findings indicate that MG132-induced ER stress, along with PERK and GCN2 activation, enhanced eIF2α phosphorylation, thereby causing a global translational shutoff of hepatic protein. CYP3A immunoprecipitation analyses of these ^{35}S-labeled cell lysates from untreated and MG132-treated hepatocytes followed by SDS-PAGE and PhosphorImager scanning revealed inhibited ^{35}S-incorporation into CYP3A

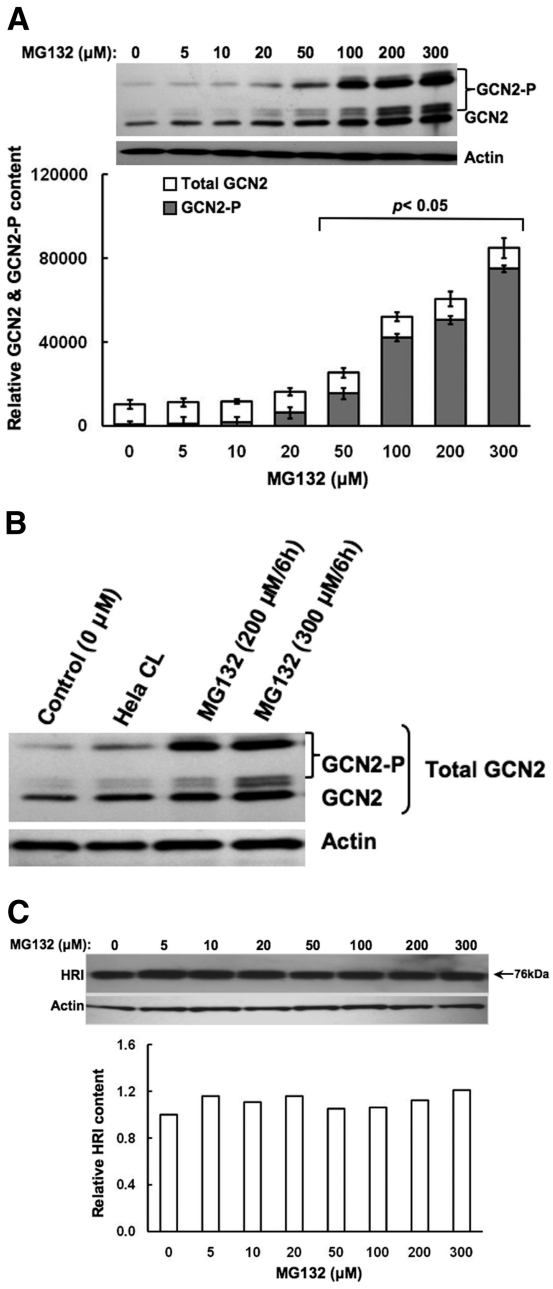

Fig. 4. Concentration-dependent effects of MG132 on induction of GCN2 content and HRI content and/or their autophosphorylation in cultured rat hepatocytes. A, rat hepatocyte cultures were treated with 0 to 300 μM MG132 as detailed. A representative example of Western immunoblotting analyses of RHL from three separate experiments (the same SDS-PAGE buffer solubilized RHL used for PERK immunoblotting analyses in Fig. 3A) is shown at the top along with corresponding aliquots used for actin immunoblotting analyses as loading controls. The densitometric quantitation of the relative GCN2-P content (solid bars; hyperphosphorylated forms ranging from 150 to 206 kDa) to the total immunochemically detectable GCN2 content (open bars) in each experiment is shown at the bottom. Values represent mean ± S.D. of at the least three separate experiments. Statistically significant differences in GCN2-P content and the GCN2-P/GCN2 values were observed at $p < 0.05$ for the 20 to 300 μM and 50 to 300 μM MG132 treatments, respectively. B, the specificity of the anti-GCN2 antibodies was verified against lysates (250 ng of GCN2 protein) from HeLa cells (CL) overexpressing GCN2, in immunoblotting analyses of lysates (50 μg of protein) from hepatocytes treated with 0, 200, or 300 μM MG132 as detailed in A. C, rat hepatocyte cultures were treated with 0 to 300 μM MG132 as detailed. A representative example of Western immunoblotting analyses of RHL (50 μg of protein) from two separate experiments is shown at the top with corresponding aliquots used for actin immunoblotting analyses as loading controls. The densitometric quantitation of the HRI content (band ≈ 76 kDa) is shown at the bottom, as an average value obtained from two separate experiments. Phosphorylated HRI is usually observed at 92 kDa. No bands above 76 kDa were observed in these immunoblots.

protein that was also particularly marked at the higher 200 to 300 μM MG132 concentrations (Fig. 6B). At the lower MG132 concentrations (10 and 20 μM), a lesser extent of inhibition was observed (Fig. 6B). The presence of HMM ^{35}S-labeled CYP3A species in hepatocytes treated with 0 to 20 μM MG132 concentrations indicated that although de novo CYP3A synthesis does occur, some newly synthesized CYP3A is also subject to ubiquitination and accumulates after proteasomal inhibition (Fig. 6B). When these ^{35}S-labeled CYP3A immunoprecipitates were quantified by liquid scintillation counting that would reflect both parent (55 kDa) and HMM species, a concentration-dependent inhibition of de novo CYP3A synthesis was observed (Fig. 6C). Thus not only is this CYP3A synthesis >90% decreased at the higher 200 to 300 μM MG132 concentrations but it is also significantly reduced even at the lower (10 and 20 μM) concentrations (Fig. 6C).

Concentration-Dependent effects of MG132 on TDO Content in Cultured Rat Hepatocytes. To determine the potential physiological relevance of this global protein suppression, we examined the concomitant effects of MG132 on the content of hepatic cytosolic TDO, the rate-limiting enzyme in hepatic tryptophan catabolism (Fig. 7). This enzyme controls tryptophan flux into serotonergic pathways in the CNS and ANS, and thus is physiologically relevant. Similar concentration-dependent MG132-induced TDO suppression was observed (Fig. 7). Together these findings indicate that after 6 h of MG132 treatment, global hepatic protein synthesis, including that of CYP3A, TDO, and Grp78, is inhibited in a concentration-dependent manner.

Concentration-Dependent Effects of MG132 on Hepatic Total Protein and CYP3A Degradation. MG132 was previously reported to reduce CYP3A4 protein stability in HepG2 cells as a result of oxidative stress stemming from a MG132-impaired NFκB activation (Zangar et al., 2008). However, such reduced CYP3A4 protein stability (i.e., enhanced degradation) was monitored by immunoblotting analyses. We reasoned that if CYP3A synthesis were being concomitantly inhibited, immunoblotting analyses would not

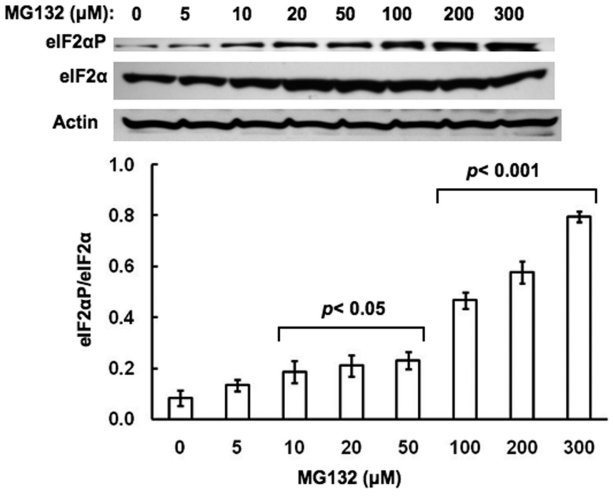

Fig. 5. Concentration-dependent effects of MG132 on eIF2αP content relative to the total hepatic eIF2α content in cultured rat hepatocytes. Rat hepatocyte cultures were treated with 0 to 300 μM MG132 as detailed. A representative example of Western immunoblotting analyses of RHL (10 μg of protein) from three separate experiments is shown at the top, with actin used as a protein loading control. The densitometric quantitation of the relative eIF2αP/total eIF2α content in each experiment is shown at the bottom. Values represent the mean ± S.D. derived from the same individual experiments depicted in Figs. 1 and 3 to 5. Statistically significant differences in the eIF2αP/total eIF2α ratios were observed at $p < 0.05$ for the 10 to 50 μM and at $p < 0.001$ for the 100 to 300 μM MG132 treatments.

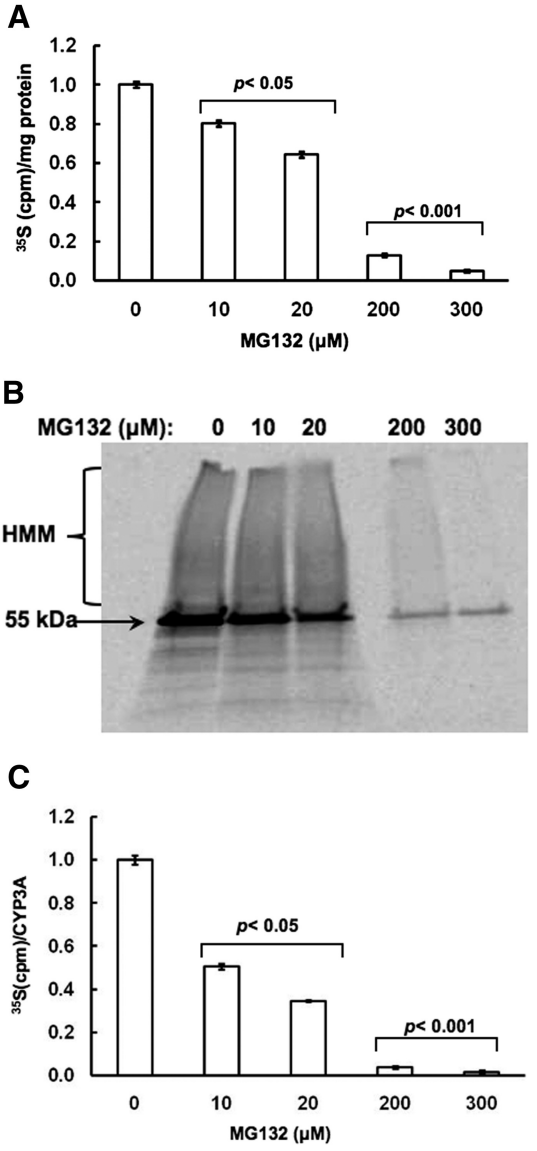

Fig. 6. Concentration-dependent effects of MG132 on de novo total protein and CYP3A syntheses in cultured rat hepatocytes. A, rat hepatocyte cultures were treated with 0, 10, 20, 200, and 300 μM MG132 as detailed. Pulse-chase analyses to monitor de novo total protein synthesis at each concentration was carried out as detailed under *Materials and Methods.* Values are depicted as mean ± S.D. from at the least three separate experiments and are expressed relative to the basal rate observed in the corresponding untreated (0 μM MG132) RHL. Statistically significant differences were observed at $p < 0.05$ for the MG132 (10 and 20 μM)-treated RHL, and at $p < 0.001$ for the MG132 (200 and 300 μM)-treated RHL. B, aliquots from the corresponding pulse-chased RHL (B) were used for CYP3A immunoprecipitation analyses. A representative PhosphorImager scan of corresponding aliquots subjected to SDS-PAGE is shown. C, quantitation of ^{35}S incorporated into CYP3A immunoprecipitates per hour is shown. Values depicted are mean ± S.D. from at the least three separate experiments and are expressed relative to the basal rate observed in the CYP3A-immunoprecipitate from the corresponding untreated (0 μM MG132) RHL. Statistically significant differences from basal value were observed at $p < 0.05$ for the CYP3A immunoprecipitate from MG132 (10 and 20 μM)-treated RHL and at $p < 0.001$ for the CYP3A immunoprecipitate from MG132 (200 and 300 μM)-treated RHL.

adequately reflect CYP3A degradation. Therefore, we monitored CYP3A degradation by pulse-chase analyses. Unlike the studies monitoring de novo CYP3A synthesis, in these studies hepatocytes were first pulsed with ^{35}S-Met/Cys for 1 h and then, at the time of chase, treated with MG132 (0, 10, 20, 200, and 300 μM) concentrations. Their degradation was followed at 3 and 8 h after pulse-chase in the presence of indicated MG132 concentrations. CYP3A immunoprecipitation analyses from lysates obtained at these times points, revealed a time-dependent reduction of ^{35}S-labeled protein in untreated hepatocytes, which was significantly blocked also in a MG132 concentration-dependent manner (Fig. 8). Thus, these results reveal that MG132 even at the higher concentrations that significantly block de novo hepatic protein and CYP3A syntheses (Fig. 6), also blocks the degradation of the ^{35}S-labeled CYP3A fraction synthesized in the absence of any MG132 during the initial hour of the pulse-chase (Fig. 8).

Confocal Immunofluorescence Microscopic Analyses of MG132-Treated Hepatocytes. Cultured hepatocytes treated with MG132 (0, 10, 20, 200, and 300 μM) concentrations were fixed, permeabilized, and treated with anti-CYP3A IgGs, followed by an Alexa Fluor 488-conjugated secondary antibody (Fig. 9). Abundant CYP3A was detected in MG132-untreated hepatocytes spread throughout the cytosol in the typical ER reticular pattern, consistent with Dex-mediated CYP3A induction (Fig. 9). Treatment with MG132 at the lower concentrations (10 and 20 μM) led to some CYP3A accumulation (Fig. 9). Furthermore, after the 20 μM treatment, a distinct perinuclear as well as plasma membrane CYP3A relocalization was detected (Fig. 9). It is unclear whether this CYP3A at the plasma membrane was intracellularly or extracellularly exposed. By contrast, a marked reduction of hepatic CYP3A levels was observed after a 6-h treatment at the higher 200 to 300 μM MG132 concentrations (Fig. 9), consistent with a corresponding marked reduction in CYP3A synthesis (Fig. 6C) and immunochemically detectable CYP3A protein (Fig. 1).

Effects of MG132 on Hepatocellular Necrosis and Apoptosis. The marked suppression of several hepatic proteins, including CYP3A, at these relatively high MG132 concentrations, led us to probe whether this suppression stemmed from MG132-induced irreversible hepatocellular damage and necrosis. Trypan Blue exclusion assays of cells treated with

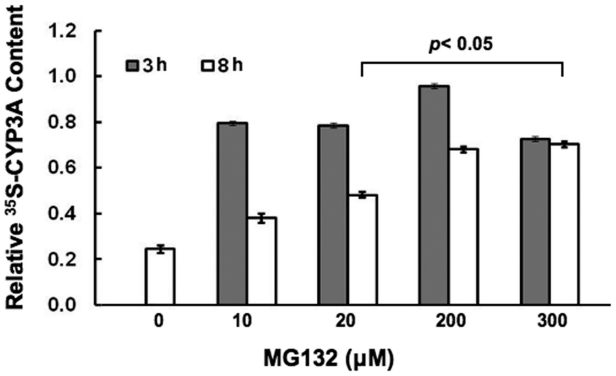

Fig. 8. Concentration-dependent effects of MG132 on CYP3A protein degradation by pulse-chase analyses in cultured rat hepatocytes. Rat hepatocyte cultures were treated with 0, 10, 20, 200, and 300 μM MG132 for 0, 3, or 8 h after pulse-chase analyses to monitor CYP3A degradation at each concentration as detailed under *Materials and Methods*. Aliquots from the corresponding pulse-chased RHL were used for CYP3A immunoprecipitation analyses. Aliquots of CYP3A-immunoprecipitates were quantified for ^{35}S-radioactivity remaining at 3 or 8 h after treatment at each MG132 concentration. Values depicted are mean ± S.D. from at the least three separate experiments and are expressed relative to the basal value observed in the CYP3A immunoprecipitate from the corresponding untreated (0 μM MG132) RHL at 0 h. Statistically significant differences from basal 0-h value were observed at $p < 0.05$ for the CYP3A immunoprecipitates from RHL treated with MG132 (20, 200, and 300 μM) for 8 h.

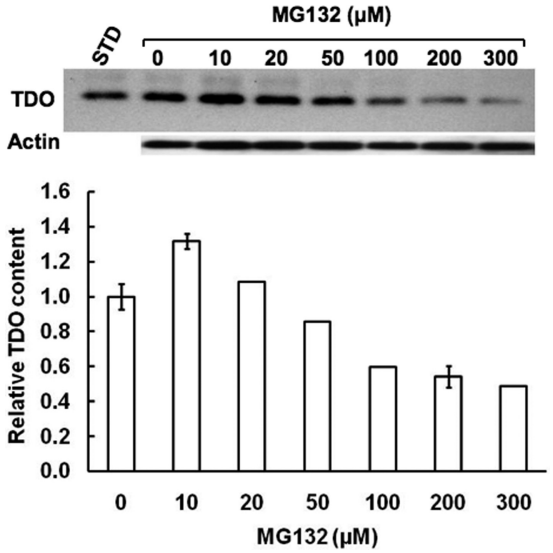

Fig. 7. Concentration-dependent effects of MG132 on hepatic TDO content. Aliquots of lysates (20 μg of protein) from hepatocytes treated with 0, 10, 20, 50, 100, 200, and 300 μM MG132 along with a purified recombinant rat liver TDO (1 pg of protein) as a standard (STD) were also subjected to immunoblotting analyses with rabbit polyclonal anti-TDO IgGs as detailed (Liao et al., 2007). Corresponding aliquots were used for actin immunoblotting analyses as loading controls. Values at 0, 10, and 200 μM MG132 concentrations represent mean ± S.D. of three individual RHL.

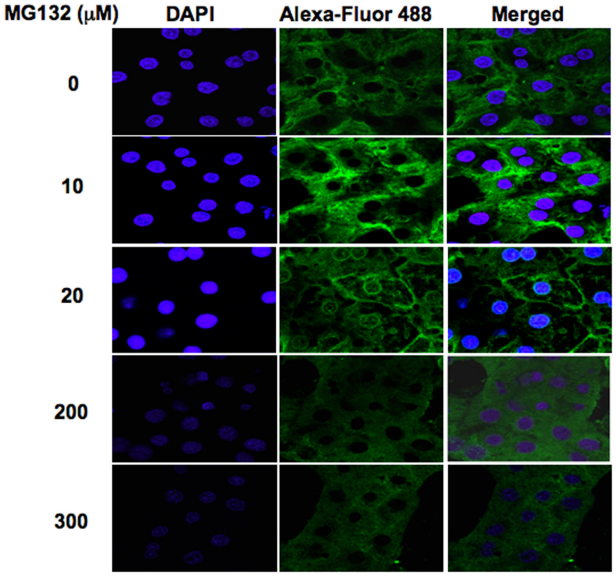

Fig. 9. Confocal immunofluorescence CYP3A protein analyses of cultured rat hepatocytes treated with MG132. Rat hepatocyte cultures were treated with 0, 10, 20, 200, and 300 μM MG132 for 8 h. After cross-linking, treated and untreated rat hepatocyte cultures were fixed and simultaneously stained with antibodies to CYP3A (green) and DAPI stain for nuclei (blue). Data including the superimposed images from a representative experiment show CYP3A accumulation at 10 μM and perinuclear/plasma membrane relocalization at 20 μM. A low-grade diffuse green signal throughout the cell body reveals marked loss of CYP3A protein at 200 and 300 μM concentrations. Higher magnification of these panels is shown in Supplemental Figure S3.

MG132 (0–300 μM) for 6 h showed a minimal statistically insignificant drop in cell viability from 99.8 ± 2.1 for untreated cells to 96.4 ± 4.1% for those treated with the higher MG132 (200 and 300 μM) concentrations (Fig. 10A). This loss was normalized to 98.1 ± 4.3% 24 h after the initial treatment with MG132 (200 μM) for 6 h. When hepatic AK release into the extracellular medium was used as a more sensitive biochemical probe of hepatic cell damage (Fig. 10B), ≈ 2% of hepatic AK was detected at MG132 concentrations of 0 to 20 μM, and this AK release into the medium was slightly increased to <15% after 6-h treatment with the higher 100 to 300 μM concentrations (Fig. 10B). But this slight extracellular AK spillage was largely abolished when after initial MG132 (200 μM) treatment for 6 h, cells were monitored in the absence of MG132 at 24 and 48 h (Fig. 10B). Together, these results reveal that the hepatic CYP3A suppression observed at the higher MG132 concentrations is not due to irreversible cell damage and/or necrotic cell death.

Proteasomal inhibition with consequent ER stress induction and enhanced eIF2α phosphorylation is well known to induce apoptosis via induced expression of the transcriptional regulator ATF4 and its target gene *CHOP*, a proapoptotic transcriptional regulator (Harding et al., 2003; Jiang et al., 2004; Jiang and Wek, 2005a). Fluorescence microscopy with higher contrast/illumination of the DAPI-stained nuclei of cells treated at the higher MG132 (200 and 300 μM) concentrations (Fig. 9) revealed some minor chromatin perturbation at 6 h of treatment with 300 μM MG132 (Supplemental Fig. S3). However, none of the prototypic morphological hallmarks of apoptosis, such as chromatin condensation, collapse, or budding and/or nuclear shrinkage or fragmentation (Martelli et al., 2001; Ziegler and Groscurth, 2004) were detected at this time (Supplemental Fig. S3). Indeed, measurement of the nuclear diameter in untreated cells and cells treated with MG132 (300 μM) (Fig. 9) revealed comparable values of 2.66 ± 0.23 and 2.63 ± 0.24 μm, respectively. However, when double-stranded DNA extracted from cells treated with MG132 (0–300 μM) concentrations was assayed for internucleosomal fragmentation, another major hallmark of nuclear apoptosis, the characteristic 180- to 200-base pair DNA fragment ladder was detected to a limited extent in cells treated with the higher MG132 (100–300 μM) concentrations at 6 h. This MG132 (200 μM)-induced profile largely subsided when cells were cultured for longer periods (24 and 48 h) after removal of MG132 from the medium (Fig. 10C). These findings using a more sensitive biochemical index of nuclear apoptosis are entirely consistent with the well recognized and therapeutically exploited effects of proteasomal inhibitors as inducers of ER stress-mediated apoptosis (Wagenknecht et al., 2000; Jiang and Wek, 2005a). However, although such signs of MG132-induced apoptosis were observed at earlier times of treatment, they were short-lived and dependent on its presence in the medium.

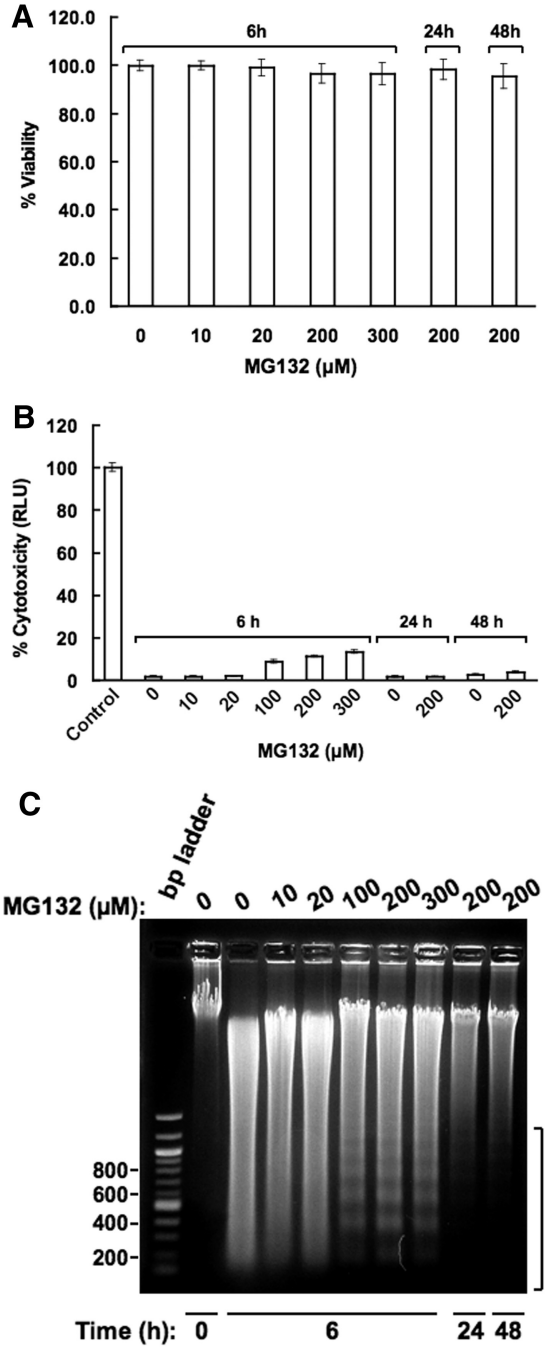

Fig. 10. MG132 effects on cell viability, extracellular AK release and hepatic DNA fragmentation in cultured hepatocytes. A, hepatocytes were treated with MG132 for 6 h as detailed and their viability was assessed by the Trypan Blue exclusion assay as described under *Materials and Methods*. Untreated and MG132 (200 μM)-treated hepatocytes were also examined after 24 and 48 h from the initiation of the treatment but after MG132 withdrawal at 6 h. Data shown are the mean ± S.D. of triplicate samples. There was no statistically significant difference in cell viability between the untreated and MG132-treated cells. B, corresponding AK release into the culture medium was assayed by the ToxiLight Assay kit as described under *Materials and Methods*. Values represent mean ± S.D. of three separate cell cultures each treated with the indicated MG132 concentration. C, total nuclear DNA was extracted and subjected to agarose gel chromatography in the presence of ethidium bromide as described previously under *Materials and Methods*. A DNA ladder was included in parallel as a standard. A representative of one experiment conducted after MG132 (0–300 μM) treatment of hepatocytes for 6 h is shown. Similar analyses of DNA extracted from cells harvested at 24 and 48 h after initial 6 h treatment with MG132 (200 μM) are also shown.

Discussion

The findings detailed above clearly document that the proteasome inhibitor MG132, depending on its specific concentration, can markedly and simultaneously reduce both hepatic CYP3A synthesis and degradation. Because of their opposing nature, the overall effects on immunochemically detectable hepatic CYP3A levels would depend on the pre-

dominant pathway under a given experimental condition. The evidence presented supports a biphasic effect on CYP3A levels monitored by immunoblotting and confocal immunofluorescence analyses. It confirms previous reports (Wang et al., 1999; Faouzi et al., 2007; Szczesna-Skorupa and Kemper, 2008) by clearly documenting that at the lower concentrations, MG132 indeed stabilizes CYP3A content, whether monitored by immunoblotting, immunofluorescence, or pulse-chase coupled with CYP3A immunoprecipitation analyses. However, pulse-chase analyses of CYP3A ^{35}S-labeled *before* MG132 treatment, also indicated that this ^{35}S-labeled CYP3A fraction was stabilized even at the higher MG132 concentrations (Fig. 8), when de novo CYP3A synthesis is almost completely shut down. This MG132-induced CYP3A stabilization is thus entirely consistent with a classic ERAD process for CYP3A turnover, wherein UPD is its principal proteolytic pathway. Thus, rigorous documentation of MG132-mediated inhibition of hepatic CYP3A UPD and its consequent protein stabilization requires either pulse-chase analyses or much lower concentrations of proteasome inhibitors, particularly when monitored by immunoblotting analyses.

Similar CYP3A stabilization at MG132 (10 μM) was also recently documented in COS1 and HepG2 cells (Szczesna-Skorupa and Kemper, 2008). It is noteworthy that in that study, as in ours (Fig. 9), CYP3A was also found to exhibit perinuclear accumulation and plasma membrane migration after 18 h of MG132 treatment. This ER to plasma membrane migration was apparently dependent on nocodazole-sensitive microtubular network (Szczesna-Skorupa and Kemper, 2008).[3] The cause for this MG132-elicited cellular P450 relocalization is unclear.

Concomitantly, MG132 treatment of hepatocytes for 6 h also progressively induced ER stress in a concentration-dependent fashion. This ER stress was signaled by a marked induction of hepatic PERK eIF2α kinase content and its functional activation via autophosphorylation, along with significantly increased content of the ER stress marker Grp78, particularly obvious at the lower MG132 concentrations (Fig. 3C). In addition, MG132 concentration-dependent induction and autophosphorylation of hepatic GCN2 were also observed (Fig. 4). The latter are consistent with a similar proteasome inhibitor-elicited GCN2 autoactivation in MEFs (Jiang and Wek, 2005a). Thus, not surprisingly, this dual hepatic PERK and GCN2 autoactivation elicited by progressively increasing MG132 concentrations dramatically enhanced hepatic eIF2α phosphorylation, with consequent global translational arrest of de novo hepatic protein syntheses. Accordingly, the de novo synthesis of hepatic ER-bound CYP3A and cytosolic TDO were impaired in parallel. Furthermore, the observed biphasic Grp78-profile reveals that such MG132-elicited translational arrest may also have reduced Grp78 content (Fig. 3C). Thus, despite the prevailing ER stress, the synthesis of this ER stress marker may also have been significantly impaired at the higher MG132 concentrations. At these high MG132 concentrations, the cell is apparently incapable of ushering the full extent of protective, stress-counteractive responses and thus becomes vulnerable to cytotoxic and/or apoptotic signals, as the increased nuclear DNA fragmentation attests (Fig. 10C).[4]

Together, our findings account for the profound CYP3A suppression by MG132 at 200 μM concentrations detected by immunoblotting analyses (Zangar et al., 2003, 2008). They also rationalize the differential CYP3A4 suppression observed over 6 h between treatment with the NFκB activation inhibitor 6-amino-4-(4-phenoxyphenyl-ethylamino)quinazoline (40%) and that with MG132 plus cycloheximide (75%) (Zangar et al., 2008). Cycloheximide is known to markedly induce eIF2α phosphorylation and to synergize the effects of ER stress inducers in MEFs (Jiang et al., 2003). Cotreatment with this protein synthesis inhibitor would thus further aggravate the gravely impaired hepatic protein synthetic capacity and lead to further "CYP3A4" suppression. It is clear that MG132-mediated inhibition of CYP3A protein synthesis occurs,[5] is quite significant at high concentrations, and needs to be either obviated or circumvented to unmask its concurrent UPD inhibition, particularly when degradation is monitored via immunoblotting analyses.

Proteasome-inhibitors, including MG132 and lactacystin, reportedly induce a heat-shock response in Madin-Darby canine kidney cells that is characterized by induction of ER chaperones Grp78/BiP, Grp94, and ERp72 and cytosolic Hsp70 chaperones (Bush et al., 1997), rendering the cells thermotolerant to subsequent relatively high heat stimuli. Furthermore, gene expression profiling after treatment with MG132, lactacystin, or its β-lactone revealed that many stress-related genes and transcription factors are induced, their salient common feature being inhibited proteasomal function (Zimmermann et al., 2000). Proteasomal inhibition results in cellular overload and consequent accumulation and/or aggregation of proteins otherwise destined for UPD clearance. Not surprisingly, the cell responds to this overload by rapidly shutting down translation of new proteins, thereby acquiring additional time to repair the damage while conserving energy and nutrients that enable it to cope with the insult.

As discussed, this prompt translational arrest in response to proteasomal inhibition is conveniently martialed through the activation of one or more of the four cellular eIF2α ki-

[3] This CYP3A at the plasma membrane was found oriented intracellularly toward the cytosol, rather than extracellularly, as documented for several other P450s (Loeper et al., 1993; Neve and Ingelman-Sundberg, 2000).

[4] In this context, it is worth noting on the one hand that proteasomal inhibitor-induced eIF2α phosphorylation is the initial event that results in the suppression of protein translation and, on the other, apoptosis via delayed translational reinitiation at upstream open reading frames results in the enhanced expression of apoptotic bZip regulators such as ATF4, CHOP, and ATF3 (Harding et al., 2002; Jiang et al., 2004; Jiang and Wek, 2005a). Thus, CYP3A suppression and apoptosis are two distinct manifestations of MG132-induced eIF2α phosphorylation. This is underscored by the much lower MG132 concentrations required to suppress CYP3A synthesis (Fig. 6C) than those required to induce DNA fragmentation (Fig. 10C).

[5] Our results, however, do not fully explain the 40% inhibition of protein synthesis observed at a 5 μM MG132 concentration in primary rat hepatocytes (Noreault-Conti et al., 2006). It is unclear whether this discrepancy is due to rat strain differences (i.e., Fisher 344 strain versus Sprague-Dawley strain) or to the fact that in that study, the hepatocytes were plated on Matrigel with no overlay, whereas ours were plated on collagen-coated Permanox plates with a Matrigel overlay. Such hepatocyte sandwich cultures would significantly protect cells from stresses, including oxidative stress due to direct exposure to 95% air. It is conceivable that differences in stress predisposition and/or relative ER stress levels may explain this discrepancy. It is noteworthy, however, that in certain cells, as little as 0.1 μM MG132 can activate UPR and PERK, resulting in eIF2α phosphorylation and consequent inhibition of de novo protein synthesis (Nishitoh et al., 2002; Jiang and Wek, 2005a).

nases: PERK, GCN2, HRI, and PKR (EIF2AK2).[6] This functional eIF2α kinase activation occurs through autophosphorylation, which in turn enhances the phosphorylation of the α-subunit of eIF2 (eIF2αP). Elevated cellular eIF2αP levels can in turn sequester eIF2B, the guanine nucleotide exchange factor that catalyzes eIF2-GDP to eIF2-GTP recycling required for translational initiation. The consequent reduction of eIF2-GTP levels results in global translational arrest, allowing cells to conserve important resources and to usher a stress remediation program to repair and/or contain the damage and return to normalcy. Although each of these cellular eIF2α kinases has a primary function specified by the nature of the particular stress or insult, each can also play a backup role, when the protagonist is functionally compromised or genetically knocked out (Jiang and Wek, 2005a). Furthermore, each cell may also determine which specific eIF2α kinase is its primary responder to a particular stress. Thus, MG132 autoactivates/induces both PERK and GCN2 in hepatocytes (Figs. 3 and 4), whereas it primarily activates PERK in PC12 cells (Nishitoh et al., 2002) and GCN2 in MEFs (Jiang and Wek, 2005a). Likewise, the proteasome inhibitor PS431 (bortezomib) also principally activates PERK in human head and neck squamous cell carcinoma cells (Fribley et al., 2004). More intriguingly, MG132 (50 μM) treatment of wild-type MEFs resulted in eIF2α phosphorylation and inhibition of protein synthesis that was unaffected in PERK(−/−), GCN2(−/−), or PKR(−/−) MEFs but was significantly impaired in HRI(−/−) (Yerlikaya et al., 2008), leading to the proposal that HRI is the principal eIF2α kinase involved in this response. However, our immunoblotting analyses indicate that MG132-induced proteasomal inhibition failed to affect hepatic HRI (Fig. 4), which is otherwise effectively activated in hepatocytes by heme depletion (Han et al., 2005; Liao et al., 2007).

ER stress-mediated activation of PERK and nutrient deprivation- or UV irradiation-mediated activation of GCN2 in MEFs result in enhanced activation of the transcription factor NFκB (Jiang et al., 2003; Wek et al., 2006). This NFκB activation is firmly associated with their eIF2α phosphorylation, as it is abolished in PERK(−/−) and GCN2(−/−) MEFs. Such stress-mediated NFκB activation apparently involves enhanced NFκB translocation into the nucleus after release from its inhibitory IκB regulators with consequent transcriptional up-regulation of gene expression involved in stress-remediation and apoptosis (Jiang et al., 2003). Such NFκB unleashing in UV-stressed MEFs is due primarily to reduced IκB translation, coupled with normal IκB turnover via phosphorylation and subsequent UPD (Jiang and Wek, 2005b). In ER-stressed MEFs, it is due to UPD-independent IκB dissociation (Wek et al., 2006). It is noteworthy that inhibition of IκB UPD by MG132 (1 μM) significantly decreased UV-induced but not ER stress-induced NFκB activation (Jiang and Wek, 2005b). By contrast, treatment of HepG2 cells with higher MG132 concentrations (200 μM) effectively suppresses NFκB activation, consistent with unaltered IκBα levels but stabilization of IκB kinase complex β and IκBβ (Zangar et al., 2008). It is intriguing that at this high MG132 concentration, despite the marked PERK and GCN2 activation and attendant eIF2α phosphorylation, hepatic NFκB activation is suppressed, being subordinate largely to MG132 proteasomal inhibition. Thus, although high concentrations of proteasomal inhibitors suppress both hepatic CYP3A content and NFκB activation, our collective findings suggest that these responses apparently stem from two separate cellular effects of these agents and may not be causally related.

We believe that our findings are physiologically and pharmacologically relevant. Some proteasomal inhibitors (i.e., bortezomib) are used clinically as apoptotic inducers for multiple myeloma therapy and are being considered for various other cancers (Nalepa et al., 2006; Voorhees and Orlowski, 2006). Other proteasomal inhibitors that are even more efficacious are being developed for diverse therapeutic strategies. Through similar protein suppression, such drugs could functionally impair hepatic P450s and other drug metabolizing enzymes and consequently result in clinically relevant DDIs in patients possibly already compromised by multiple drug therapy. Furthermore, MG132-induced suppression of hepatic TDO, an enzyme that controls circulating tryptophan levels and thus the central nervous system/autonomic nervous system serotonergic tone reveals that these agents can also target physiologically relevant pathways. More importantly, these findings suggest that caution is warranted with their dosage regimens because significant hepatic protein translational arrest occurs even at 10 μM (Fig. 6A). Depending on the specific proteins slated for translational arrest at this low concentration, various other vital hepatic physiological pathways may also be compromised at otherwise therapeutic concentrations of these drugs.

Acknowledgments

We thank Prof. Ronald C. Wek (Indiana University, Indianapolis, IN) for providing a GCN2 antibody used in preliminary studies. We also thank Ali Naqvi and Theresa Canavan, UCSF Liver Center Cell and Tissue Biology Core Facility (Dr. J. J. Maher, Director) for hepatocyte isolation and elutriation. We also gratefully acknowledge Dr. Ed LeCluyse and Rachel Whisnant (CellzDirect) for generously providing the human hepatocytes used in these studies.

References

Berlanga JJ, Santoyo J, and De Haro C (1999) Characterization of a mammalian homolog of the GCN2 eukaryotic initiation factor 2alpha kinase. *Eur J Biochem* **265:**754–762.

Bush KT, Goldberg AL, and Nigam SK (1997) Proteasome inhibition leads to a heat-shock response, induction of endoplasmic reticulum chaperones, and thermotolerance. *J Biol Chem* **272:**9086–9092.

Correia MA, Sadeghi S, and Mundo-Paredes E (2005) Cytochrome P450 ubiquitination: branding for the proteolytic slaughter? *Annu Rev Pharmacol Toxicol* **45:**439–464.

Faouzi S, Medzihradszky KF, Hefner C, Maher JJ, and Correia MA (2007) Characterization of the physiological turnover of native and inactivated cytochromes P450 3A in cultured rat hepatocytes: a role for the cytosolic AAA ATPase p97? *Biochemistry* **46:**7793–7803.

Fribley A, Zeng Q, and Wang CY (2004) Proteasome inhibitor PS-341 induces apoptosis through induction of endoplasmic reticulum stress-reactive oxygen species in head and neck squamous cell carcinoma cells. *Mol Cell Biol* **24:**9695–9704.

Han XM, Lee G, Hefner C, Maher JJ, and Correia MA (2005) Heme-reversible impairment of CYP2B1/2 induction in heme-depleted rat hepatocytes in primary culture: translational control by a hepatic alpha-subunit of the eukaryotic initiation factor kinase? *J Pharmacol Exp Ther* **314:**128–138.

Harding HP, Calfon M, Urano F, Novoa I, and Ron D (2002) Transcriptional and translational control in the mammalian unfolded protein response. *Annu Rev Cell Dev Biol* **18:**575–599.

Harding HP, Zhang Y, Zeng H, Novoa I, Lu PD, Calfon M, Sadri N, Yun C, Popko B, Paules R, et al. (2003) An integrated stress response regulates amino acid metabolism and resistance to oxidative stress. *Mol Cell* **11:**619–633.

Jiang HY and Wek RC (2005a) Phosphorylation of the alpha-subunit of the eukaryotic initiation factor-2 (eIF2alpha) reduces protein synthesis and enhances apoptosis in response to proteasome inhibition. *J Biol Chem* **280:**14189–14202.

Jiang HY and Wek RC (2005b) GCN2 phosphorylation of eIF2alpha activates NF-kappaB in response to UV irradiation. *Biochem J* **385:**371–380.

[6] Double-stranded RNA-activated PKR is usually induced by viral inducers or class 1 interferons that were not specifically included in the cell culture; it therefore was not examined.

Jiang HY, Wek SA, McGrath BC, Scheuner D, Kaufman RJ, Cavener DR, and Wek RC (2003) Phosphorylation of the alpha subunit of eukaryotic initiation factor 2 is required for activation of NF-kappaB in response to diverse cellular stresses. *Mol Cell Biol* **23:**5651–5663.

Jiang HY, Wek SA, McGrath BC, Lu D, Hai T, Harding HP, Wang X, Ron D, Cavener DR, and Wek RC (2004) Activating transcription factor 3 is integral to the eukaryotic initiation factor 2 kinase stress response. *Mol Cell Biol* **24:**1365–1377.

Korsmeyer KK, Davoll S, Figueiredo-Pereira ME, and Correia MA (1999) Proteolytic degradation of heme-modified hepatic cytochromes P450: A role for phosphorylation, ubiquitination, and the 26S proteasome? *Arch Biochem Biophys* **365:**31–44.

LeCluyse E, Bullock P, Madan A, Carroll K, and Parkinson A (1999) Influence of extracellular matrix overlay and medium formulation on the induction of cytochrome P-450 2B enzymes in primary cultures of rat hepatocytes. *Drug Metab Dispos* **27:**909–915.

Lee AH, Iwakoshi NN, Anderson KC, and Glimcher LH (2003) Proteasome inhibitors disrupt the unfolded protein response in myeloma cells. *Proc Natl Acad Sci U S A* **100:**9946–9951.

Liao M, Faouzi S, Karyakin A, and Correia MA (2006) Endoplasmic reticulum-associated degradation of cytochrome P450 CYP3A4 in Saccharomyces cerevisiae: further characterization of cellular participants and structural determinants. *Mol Pharmacol* **69:**1897–1904.

Liao M, Pabarcus MK, Wang Y, Hefner C, Maltby DA, Medzihradszky KF, Salas-Castillo SP, Yan J, Maher JJ, and Correia MA (2007) Impaired dexamethasone-mediated induction of tryptophan 2,3-dioxygenase in heme-deficient rat hepatocytes: translational control by a hepatic eIF2alpha kinase, the heme-regulated inhibitor. *J Pharmacol Exp Ther* **323:**979–989.

Loeper J, Descatoire V, Maurice M, Beaune P, Belghiti J, Houssin D, Ballet F, Feldmann G, Guengerich FP, and Pessayre D (1993) Cytochromes P-450 in human hepatocyte plasma membrane: recognition by several autoantibodies. *Gastroenterology* **104:**203–216.

Lown KS, Bailey DG, Fontana RJ, Janardan SK, Adair CH, Fortlage LA, Brown MB, Guo W, and Watkins PB (1997) Grapefruit juice increases felodipine oral availability in humans by decreasing intestinal CYP3A protein expression. *J Clin Invest* **99:**2545–2553.

Martelli AM, Zweyer M, Ochs RL, Tazzari PL, Tabellini G, Narducci P, and Bortul R (2001) Nuclear apoptotic changes: an overview. *J Cell Biochem* **82:**634–646.

Murray BP and Correia MA (2001) Ubiquitin-dependent 26S proteasomal pathway: a role in the degradation of native human liver CYP3A4 expressed in Saccharomyces cerevisiae? *Arch Biochem Biophys* **393:**106–116.

Nalepa G, Rolfe M, and Harper JW (2006) Drug discovery in the ubiquitin-proteasome system. *Nat Rev Drug Discov* **5:**596–613.

Neve EP and Ingelman-Sundberg M (2000) Molecular basis for the transport of cytochrome P450 2E1 to the plasma membrane. *J Biol Chem* **275:**17130–17135.

Nishitoh H, Matsuzawa A, Tobiume K, Saegusa K, Takeda K, Inoue K, Hori S, Kakizuka A, and Ichijo H (2002) ASK1 is essential for endoplasmic reticulum stress-induced neuronal cell death triggered by expanded polyglutamine repeats. *Genes Dev* **16:**1345–1355.

Noreault-Conti TL, Jacobs JM, Trask HW, Wrighton SA, Sinclair JF, and Nichols RC (2006) Effect of proteasome inhibition on toxicity and CYP3A23 induction in cultured rat hepatocytes: comparison with arsenite. *Toxicol Appl Pharmacol* **217:** 245–251.

Paine MF, Widmer WW, Hart HL, Pusek SN, Beavers KL, Criss AB, Brown SS, Thomas BF, and Watkins PB (2006) A furanocoumarin-free grapefruit juice establishes furanocoumarins as the mediators of the grapefruit juice-felodipine interaction. *Am J Clin Nutr* **83:**1097–1105.

Szczesna-Skorupa E and Kemper B (2008) Proteasome inhibition compromises direct retention of cytochrome P450 2C2 in the endoplasmic reticulum. *Exp Cell Res* **314:**3221–3231.

Voorhees PM and Orlowski RZ (2006) The proteasome and proteasome inhibitors in cancer therapy. *Annu Rev Pharmacol Toxicol* **46:**189–213.

Wagenknecht B, Hermisson M, Groscurth P, Liston P, Krammer PH, and Weller M (2000) Proteasome inhibitor-induced apoptosis of glioma cells involves the processing of multiple caspases and cytochrome c release. *J Neurochem* **75:**2288–2297.

Wang HF, Figueiredo Pereira ME, and Correia MA (1999) Cytochrome P450 3A degradation in isolated rat hepatocytes: 26S proteasome inhibitors as probes. *Arch Biochem Biophys* **365:**45–53.

Wek RC, Jiang HY, and Anthony TG (2006) Coping with stress: eIF2 kinases and translational control. *Biochem Soc Trans* **34:**7–11.

Yang J, Liao M, Shou M, Jamei M, Yeo KR, Tucker GT, and Rostami-Hodjegan A (2008) Cytochrome P450 turnover: regulation of synthesis and degradation, methods for determining rates, and implications for the prediction of drug interactions. *Curr Drug Metab* **9:**384–394.

Yerlikaya A, Kimball SR, and Stanley BA (2008) Phosphorylation of eIF2alpha in response to 26S proteasome inhibition is mediated by the haem-regulated inhibitor (HRI) kinase. *Biochem J* **412:**579–588.

Zangar RC, Kocarek TA, Shen S, Bollinger N, Dahn MS, and Lee DW (2003) Suppression of cytochrome P450 3A protein levels by proteasome inhibitors. *J Pharmacol Exp Ther* **305:**872–879.

Zangar RC, Bollinger N, Verma S, Karin NJ, and Lu Y (2008) The nuclear factor-kappa B pathway regulates cytochrome P450 3A4 protein stability. *Mol Pharmacol* **73:**1652–1658.

Ziegler U and Groscurth P (2004) Morphological features of cell death. *News Physiol Sci* **19:**124–128.

Zimmermann J, Erdmann D, Lalande I, Grossenbacher R, Noorani M, and Fürst P (2000) Proteasome inhibitor induced gene expression profiles reveal overexpression of transcriptional regulators ATF3, GADD153 and MAD1. *Oncogene* **19:**2913–2920.

Address correspondence to: M. A. Correia, Dept. of Cellular and Molecular Pharmacology, Mission Bay Campus, Genentech Hall, 600 16th Street, N572F/Box 2280, University of California, San Francisco, CA 94158. E-mail: almira.correia@ucsf.edu